Processes and evolution of the Pleistocene coastal sedimentary succession of Es Codolar (Southern Eivissa, Balearic Islands, Western Mediterranean): insights from soft-sediment deformation structures

Laura del Valle[1,2] · **Francesc Pomar**[2] · **Joan J. Fornós**[2] · **Bernadí Gelabert**[2] · **Alida Timar-Gabor**[1,3]

Abstract

We analyze the evolution of the undeformed Middle to Late Pleistocene deposits of Es Codolar (Southern Eivissa, Western Mediterranean). The outcrop records a succession characterized by the alternation of aeolian, colluvial and alluvial fan deposits and palaeosols that result in a complex stratigraphic architecture. In this area, aeolian beds, colluvial deposits and palaeosols are exposed along sea-cliffs for almost 500 m, allowing detailed descriptions both of the general sedimentological and geomorphological features of the Middle to Late Pleistocene deposits. Several different types of soft-sediment deformation structures are described (load-casts structures, injection structures, water-scape structures, rizoconcretions), which will help us in the understanding of the climatic evolution and the syn- post-depositional processes. In this way, main processes triggering the formation of these structures seem to be sea level changes together with a wetter environment during warmer climatic episodes.

Keywords Eivissa · Pleistocene · Aeolianites · Soft-sediment deformation structures

Introduction

In the western Mediterranean, Pleistocene climatic changes resulted in several wet and dry periods (Martrat et al. 2004) combined with sea level fluctuations (Dorale et al. 2010). The past climate change record of Eivissa is recorded in the alternation of aeolianites and palaeosols, representing cold and warmer periods, respectively (Zazo 1999; Del Valle et al. 2015; Del Valle 2016).

✉ Laura del Valle
    laura.del-valle@uib.eu;
    DeLa14061@studmail.ubbcluj.ro

1   Faculty of Environmental Sciences and Engineering, Babes-Bolyai University, Cluj-Napoca, Romania

2   Present Address: Earth Sciences Research Group, Universitat de Les Illes Balears, Palma, Mallorca, Spain

3   Interdisciplinary Research Institute on Bio-Nano-Sciences, Babes-Bolyai University, Cluj-Napoca, Romania

Pleistocene sedimentary deposits of Eivissa (Balearic Islands), outcropping patchily along the coasts, provide an excellent record of glacial–interglacial cycles and eustatic fluctuations. The main representative deposits are the aeolianites, also present at other locations in the Balearic Islands (Clemmensen et al. 2001; Nielsen et al. 2004; Fornós et al. 2009, 2012a; Pomar 2016) and western Mediterranean (Andreucci et al. 2010, 2014; Pappalardo et al. 2013; El-Asmar 1994). The quick lithification of the aeolian deposits after subaerial exposure allows preserving a high-resolution sedimentological record (Fornós et al. 2012a, b). Sedimentary successions containing Pleistocene coastal aeolianites at Eivissa use to display wide sorts of deposits characterized by colluvial facies and palaeosols and some thin shallow marine facies interbedded. In this sense, the variety of deposits and sometimes the rugged geomorphology of the coasts show a complex architecture (Pomar et al. 2015; Del Valle et al. 2016a, b; Del Valle 2016).

The main goal of this article is to present the sedimentary and climatic evolution of the Middle to Late Pleistocene deposits of Es Codolar (Southern Eivissa, Western Mediterranean). The outcrop records a succession characterized by the alternation of aeolian, colluvial and alluvial fan deposits and palaeosols that result in a tangled stratigraphic

architecture. In this area, aeolian beds, colluvial deposits and palaeosols are exposed along sea-cliffs for almost 500 m, allowing detailed descriptions both of the general sedimentological and geomorphological features of the Middle to Late Pleistocene deposits.

The second goal of this study is to describe for the first time the presence of soft-sediment deformation structures at Es Codolar succession and its implications for the evolution of the sedimentary succession. For this reason, identified soft-sediment deformation structures are described and deformation mechanisms are proposed.

The term soft-sediment deformation refers to several processes which change and disrupt the sedimentary structures of unconsolidated sediments. Deformation usually occurs rapidly, close to the surface, during or shortly after the deposition, and before significant diagenesis (Owen et al. 2011). The soft-sediment deformation structures are widely described in the literature (e.g., Lowe 1975, 1976; Allen 1982; Mills 1983; Owen 1987, 1996; Maltman 1994). Deformations features in aeolian deposits have long been recognized in the geologic record (e.g., Allen 1982; Moretti 2000; Olabode 2014). They affect mostly multilayer deposits, especially sand-marl sequences, being concentrated along bedding planes or single beds, but they can as well spread through the whole deposit (Horváth et al. 2005). Most of them are related to a substantial decrease in shear resistance in water-saturated and unconsolidated sediments. They have been attributed to pore pressure changes most probably caused by fluid escape during fluidization and liquefaction (Lowe 1975; Allen 1982; Owen 1987; Rossetti 1999). Liquefaction and fluidization are the main processes which allow a temporary change from solid to liquid-like behavior in silts

and sands (Allen 1982). Many natural processes may induce liquefaction and fluidization such as uneven loading, overloading, wave-originated cyclical and/or impulsive stresses, sudden changes in earthquakes and water table (Allen 1982; Owen 1987, 1996; Molina et al. 1998; Rossetti 1999; Moretti 2000).

Study area

The Eivissa island is situated in the south-western Mediterranean Sea and it is considered the third largest (571 km^2) and most Westerly island of the Balearic Archipelago (Fig. 1A). Geological structure of the island consists of a series of mainly Middle Triassic to Middle Miocene carbonate deposits thrust sheets trending NE–SW (Rangheard 1971). Muschelkalk limestone and dolomite, as well as Keuper marls and clays made up the Triassic materials of the island, whereas Jurassic limestone and dolomites and Cretaceous to Middle Miocene limestone overlie the Triassic materials and comprise the major reliefs of the island (Fig. 1B). Quaternary fluvial, alluvial and colluvial sediments fill the central basins, whereas Pleistocene coastal successions characterized by beaches to littoral aeolian and colluvial deposits crop out irregularly along the cliffed coasts (Del Valle et al. 2016a). Balearic Islands have been considered tectonically stable since the Pliocene with negligible or very little tectonic movements (Fornós et al. 2012a, b; Just et al. 2011; Sàbat et al. 2011).

The outcrop of Es Codolar (38°51′01″N–1°22′03″E) is extending continuously along 500 m of coastline and approximately 300 m inland. The Pleistocene succession is
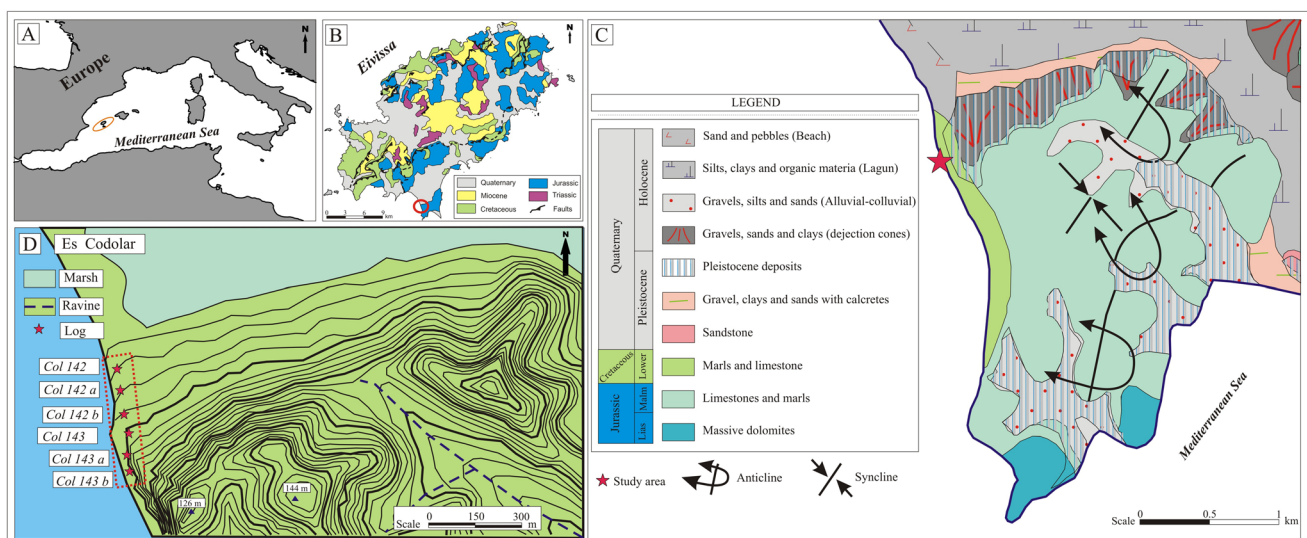
Fig. 1 A Location of the studied area; B geological map of Eivissa modified by Diaz de Neira et al. (1997); C detail of geological map of the studied area modified from Gil et al. (1997) and D topographic map and stratigraphic logs from the studied area

bounded at the base by an unconformity resting on folded upper Jurassic (Malm) marly limestones (Fig. 1C). The succession shows a complex alternation of colluvial–alluvial deposits built up by heterometric matrix to clast-supported breccias, aeolianites and red palaeosols (Del Valle 2016). Es Codolar deposits are capping the steep slopes facing northwest of Puig des Falcó (144 m) and are showing a vertical cliff seaward shaped by wave erosion (Fig. 1D).

Methods

We have conducted sedimentological analyses to identify the main facies and stratigraphic units composing the sequence. Additionally, we also have performed OSL analysis on aeolianites samples to unravel the ages of these deposits and the palaeoenvironmental context that took place during the deposition.

Facies analysis

Facies analysis has been performed acquiring additional six lithostratigraphic logs (Fig. 1D). Logs were analyzed and correlated regarding major unconformities, bounding surfaces and the lateral continuity and architecture of the deposits. Units were defined in terms of brusque/abrupt facies changes.

Information on cross-bed dip direction for paleocurrent analyses was collected. Rock samples were taken for grain size, carbonate content and mineralogical composition. Carbonate content was derived by hydrochloric acid etching by means of Bascomb calcimeter method. All collected samples showed a high degree of cementation, so they were cut and polished to perform grain size analysis. Images on polished faces were taken with a 4× binocular magnifying and Motic Image 2.0 software to make observations on grain composition and size. Sample images were analyzed by means of ImageJ open source software. For the remaining analyses, samples were crushed. The resulting powder was used to identify the color by comparing dry sample powder and Munsell charts with artificial light. Mineralogical content was analyzed through X-ray powder diffraction with the SIEMENS D5000 diffractometer using Cu Kαradiation. Diffraction spectra were recorded from 3° up to 65°2θ with lapses of 0.03° every 3 s at 25 °C and compiled in digital archives for later analysis. Using X-Powder v.2010.01.09 software, a semi-quantitative analysis was carried out comparing the results with the data base Difdata (Downs and Hall-Wallace 2003).

Soft-sediment deformation structures (SSD)

Detailed photographs of the different sections displaying deformations were taken to describe the main features. The shape and geometry of the deformations were described by means of digital image reconstructions combined with the field observations (Chan and Bruhn 2014). Classifications of soft-sediment deformation structures can be used to establish morphologic and genetic systematizations. Thus, in our study area the following characteristics were identified: limited deformations among stratigraphic horizons, lateral continuity of SSD structures at appreciable distances and a confinement between non-deformed strata and its lithological association with psammitic–pelitic deposits. Soft-sediment deformation structures identified in this study were described and classified according the works of Rossetti (1999), Moretti (2000), Horváth et al. (2005), Moretti and Sabato (2007), Shillizzi et al. (2010), KoçTaşgin et al. (2011), and Ezquerro et al. (2016).

Optically stimulated luminescence (OSL) dating

OSL dating relies on the properties of some mineral grains such as quartz, but not only, to store energy resulted from exposure to the environmental radiation field during their burial within deposits, and its later release it in the form of light upon stimulation with light under controlled laboratory conditions. OSL has become a key chronological tool of Quaternary siliciclastic successions and recent contributions have highlighted the suitability of this method for aeolian sediments such as carbonate aeolianites (Murray and Clemmensen 2000; Nielsen et al. 2004; Fornós et al. 2009; Anechitei-Deacu et al. 2018) and their possible correlation with the marine isotopic stages in order to obtain climatic information on the formation of these deposits and their geomorphological processes. The aeolianites collected at Es Codolar, contain between 1 and 8% of siliciclastic grains, primarily quartz. Three rock samples ($\sim 70 \times 70 \times 50$ cm; 6 kg) were collected for luminescence dating from aeolian deposits at Es Codolar. Aeolianite blocks were extracted from the stratigraphic layers considered to be representative of the succession. Blocks were detached in shadowed low light conditions and wrapped in lightproof material, labeled and documented and transported to the laboratory. The inner part of each sample was extracted in the laboratory and subsequently treated with HCl (30%) and H_2O_2 (10% and 30%) for carbonate and organic matter removal. The remaining material was sieved to obtain material < 63 μm and different fractions ranging from 63 to 250 μm. The mineral fraction was subsequently etched with 40% HF for 60 min.

The equivalent dose measurements were undertaken using a Risø TL/OSL-DA-20 luminescence reader (Thomsen et al. 2006). The ^{90}Sr–^{90}Y beta source was calibrated

using gamma-irradiated calibration quartz supplied by Risø National Laboratory (Hansen et al. 2015). For these measurements, the modified single aliquot regenerative protocol (Murray and Wintle 2003) was applied, with preheat of 10 s at 220 °C, a cut heat to 180 °C and an elevated temperature bleach of 40 s at 280 °C at the end of each cycle. Radionuclide concentrations were derived by high-resolution gamma spectrometry and were transformed to dose rates using published conversion factors (Adamiec and Aitken 1998). The cosmic ray contribution was evaluate using published formulae (Prescott and Hutton 1994). Water content estimation was based on the difference in weight of the material from the inner part of the blocks, before and after oven drying, assuming a relative error of 25% for the time-averaged water content.

Results

Stratigraphic succession and facies analyses

Textural and compositional analyses have enabled to differentiate four major sedimentary deposits which represent aeolian and colluvial facies and two types of palaeosols (Fig. 2).

Aeolian facies

Aeolian facies are characterized by very pale brown color (HUE 10 YR 8/2), well-sorted, fine to medium-grained sandstones, with large-scale trough cross stratification. The strata are 0.5 m–3 m thick and are moderately disrupted by root casts (0.50 a 5 cm width and 0.10–1 m in length). Most of them are remains of moulds and calcified root casts. The facies composition is mainly medium-grained carbonate marine sand with very little terrigenous material (i.e., quartz grains). As stated to the diffraction analysis, calcite is the main mineral (80%) and there is a minor presence of clay minerals. These deposits record the wind-transported marine carbonate sand trapping in front of a steep inland cliff. The aeolian levels present an active migration inland towards ESE–SE direction. High-angle cross-stratified layers have a direction of N45°/25°/SE.

Colluvial facies

Colluvial facies are characterized by massive reddish (HUE 5 YR 6/8) to pale brown (HUE 10 YR 8/3) silty matrix-supported breccias, composed of angular clasts forming millimeter to centimeter thick layers disrupted by calcrete levels. Large clasts are aligned downslope (270°–330°NW), although the clasts display modal fabric orientation. Clasts come from the erosion of the basement composed of Jurassic marly limestones. Conforming to the diffraction analysis,

the main composition is characterized by carbonates (72%). These deposits record episodic mass movements on slope surfaces characterized mainly by debris-flows transport.

Palaeosols

Two different types of palaeosols have been observed. The first one, around 20–40 cm thick is mainly composed of reddish silts (HUE 5 YR 6/8) with the presence of iron bands. According to the diffraction analysis, quartz is the main mineral (20%) and there is a minor presence of clay minerals. The second one is characterized by massive silt and silty–sandy deposits with nodular forms and lots of bioturbation evidence with some root casts. Its color is very pale brown (HUE 10 YR 8/4) and layers are 0.30–1.5 m thick, rich in carbonate (71%). These palaeosols may represent periods of warmer environments characterized by very little erosion rates on slopes and the development of vegetation.

Stratigraphic units

Es Codolar outcrop is composed of four units. Unit 1 (U1) consists of three colluvial levels interbedded with palaeosols. This unit is bounded at the base by an unconformity resting on the Jurassic basement. Thin calcretes are capping the colluvial–palaeosols sequence at the upper part.

In general, it is possible to observe three repeated sequences at U2, U3 and U4. All of them are made up from the base to the top by calcretes, palaeosol and/or colluvial deposits, aeolian deposits and palaeosol. The lower palaeosol of each unit is filling up the rizoconcretion moulds of the immediately upper sandy level (aeolian facies) (Fig. 2).

Soft-sediment deformation structures

Eleven different types of well-exposed soft-sediment deformation structures were distinguished in the Es Codolar. On characterizing the deformation structures, we considered lithology, size and geometrical characteristics (Fig. 3). Fifteen deformed levels have been observed .

Contorted structures

Contorted structure is used as a general term for all types of features with different degrees of crumpling or complicated folding of the laminae within sand beds (Brenchely and Newall 1977). It was possible to define several types of contorted stratification: small-scale slump, large-scale slump, small-scale load structures, large-scale load structures, deformed lamination, recumbent folds, convolute folds, ball and pillow, concave up path with consolidation lamination. In the study area, three deformation structures were observed: load structures and recumbent folds.
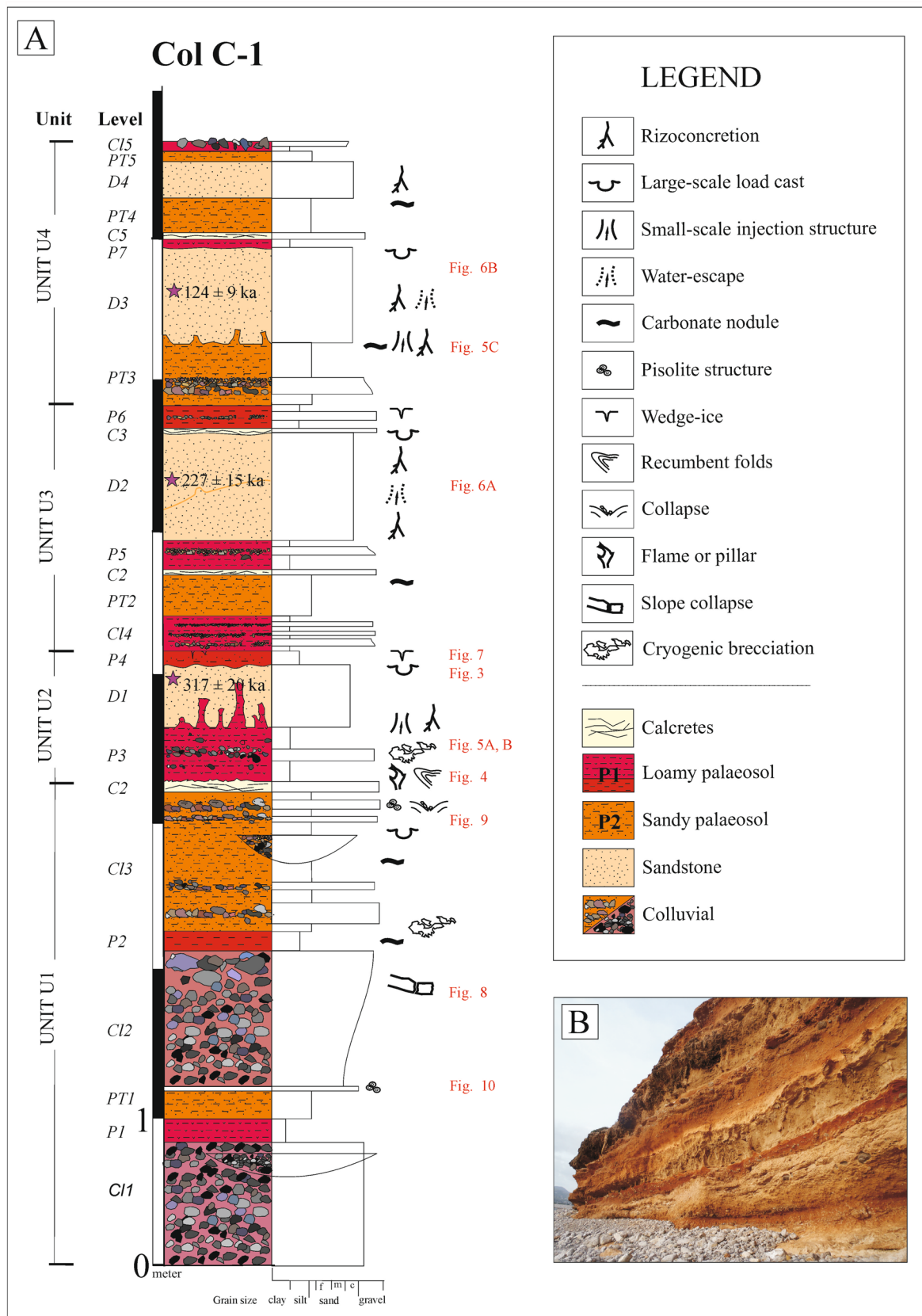
Fig. 2 **A** Lithostratigraphic log and main facies characteristic of Pleistocene Es Codolar formation. **B** Photography of the outcrop

Load structures

Load structures are laterally continuous undulations at an interface between layers that varied in density with relatively denser sediment above an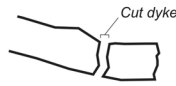d less dense below. Deformation is driven by the gravitational forces associated with the reverse density system and it is dominated by vertical displacements (Owen et al. 2011). Internal laminae are well-recognizable and, typically simulate the external circular form of the load structures (Moretti and Sabato 2007).

These forms are located in between carbonated sandstone and silts. The undulations are between 30 and 50 cm width,

	Soft-sediment deformation structures		Mechanisms deformation	Driving-force system	Trigger mechanism
CONTORNED	Load-cast		*Fluidization*	Gravitationally unstable density gradient	Overloading or periglacial loading
	Recumbent folds		*Liquefaction / fluidization*	Gravitationally unstable density gradient and action drag	Overloading or periglacial loading
INTRUDED	Injection structures		*Liquefaction*	Vertical shear stress	Bioturbation, overloading and cryohydrostatic pressure
	Water-escape structures		*Liquefaction*	Vertical shear stress and gravitationally, unstable density gradient	Overloading, cryohydrostatic pressure.
	Flames and Pillars		*Liquefaction*	Gravitationally unstable density gradient	Cryohydrostatic pressure and / or periglacial loading
	Dykes, sill-dyke, pillar		*Liquefaction / fluidization*	Gravitationally unstable density gradient	Cryohydrostatic pressure and/or periglacial loading
	Wedge-ice		*Liquefaction / cryoturbation*	Vertical body force and freezing	Periglacial loading and/or cryohydrostatic pressure
	Cryogenic brecciation		*Liquefaction / Fluidization / cryoturbation*	Vertical body force and freezing	Periglacial loading and/or cryohydrostatic pressure
BRITTLE	Slope collapse	Cut dyke	*Rugged cut slump*	Gravitational body pressure and steep slope	Action drag and overloading
	Collapse structures		*Overload*	Gravitational body pressure	Overloading and cryohydrostatic pressure

Fig. 3 Classification of the soft-sediment deformation structures described at Es Codolar succession. Different driving force systems, deformation and trigger mechanisms for each kind of soft-sediment deformation structure are presented
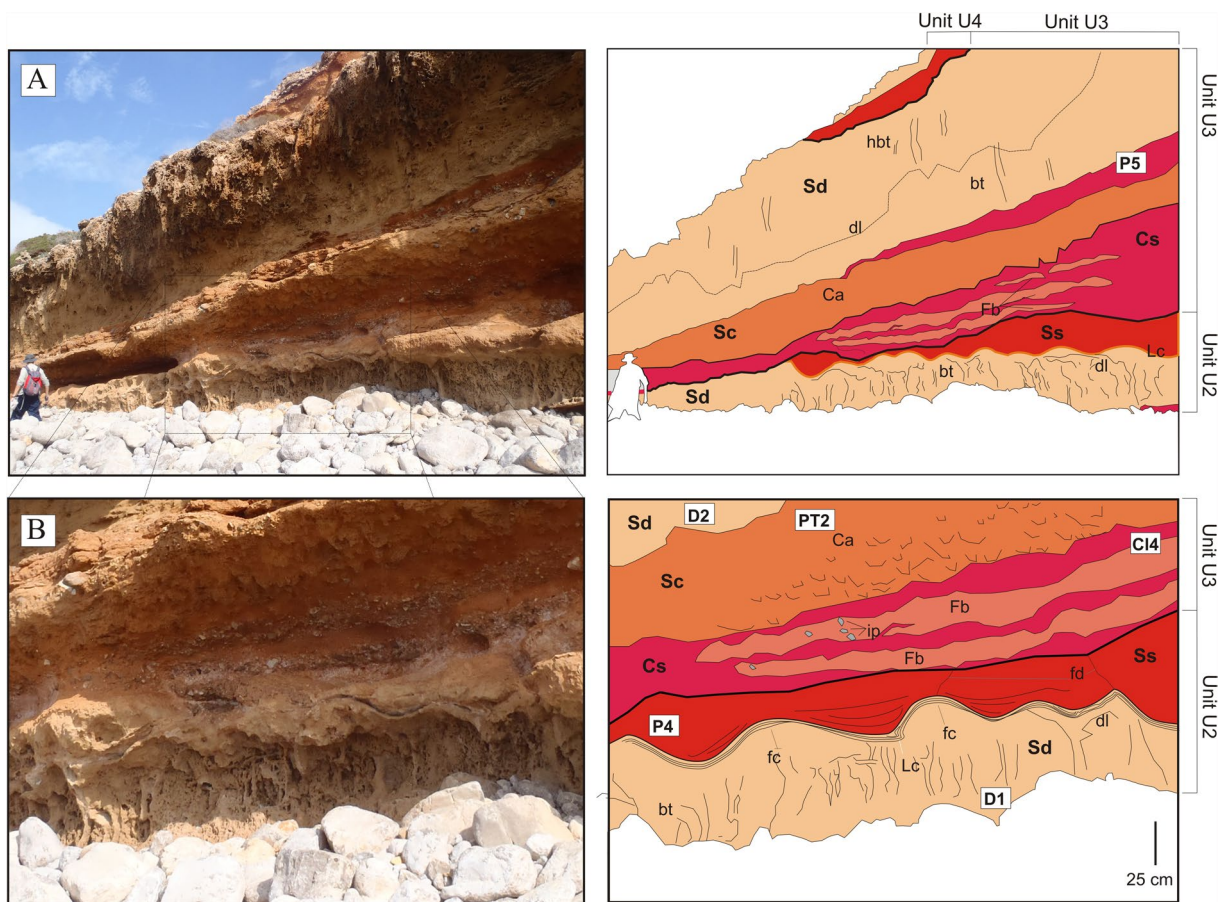
Fig. 4 A Composite picture (left) and line drawing (right) and **B** detail of the picture **A** showing flexis caves (fc), distorted lamination (dl), folded breccia (Fb), imbricated pebbles (ip) and folded dykes (fd) associated with large-scale load structures (Lc). Note the presence of bioturbation (bt), highly bioturbation (hbt) and carbonate nodules (Ca); cryogenic brecciation (Cbt). Lithological characteristics, sandstones (Sd), loamy sands (Sc) and marl (Cs). Lithostratigraphical description (see Fig. 2), first dune (D1) correspond to the unit U2, loamy palaeosol four (P4) from unit U2, colluvial four (Cl4) corresponding to the unit U3, sandy palaeosol two (PT2), loamy palaeosol five (P5) and second dune corresponding to the unit U3

and 20 cm and 30 cm high. They display a regular concave and convex morphology (wavy laminae) along the outcrop (Fig. 4). This deformation is present in all units of the outcrop within the sandstone levels, silty layers and calcretes levels. These structures extend continuously for 200 m along the coastline. The presence of deformation breccia (Fb), flexi caves (fc), convex structures with vertical axial plane characteristic by 20 cm in height and 13 cm in width is associated with these structures (Figs. 5 and 6).

Recumbent folds

These structures consist of cross-sets with overturned internal stratification, which forms recumbent folds with either horizontal or slightly inclined axial planes (Rossetti 1999). These structures were developed in cross-bedded calcretes or loamy sands. Layers under the recumbent folds show sigmoid and concave forms. Recumbent folds at the uppermost part have parabolic morphology and there is no structure on the fold limbs. Recumbent folds are 15–20 cm in height and 30 cm wide. Fold axes are sub-horizontal and generally oblique to the dip of the not deformed foresets strata. The folds have mainly rounded hinge zones. These structures can be observed at the level C2 of the Unit U1 (Fig. 5).

Intruded structures

This term is used to group sandstone or silty–clay masses displaying different styles of elongate shapes that have intruded into other soft-sediment deformation structures (Lowe 1975; Rossetti 1999). The intruded structures are either conformable or disrupt bedding (Rossetti 1999).
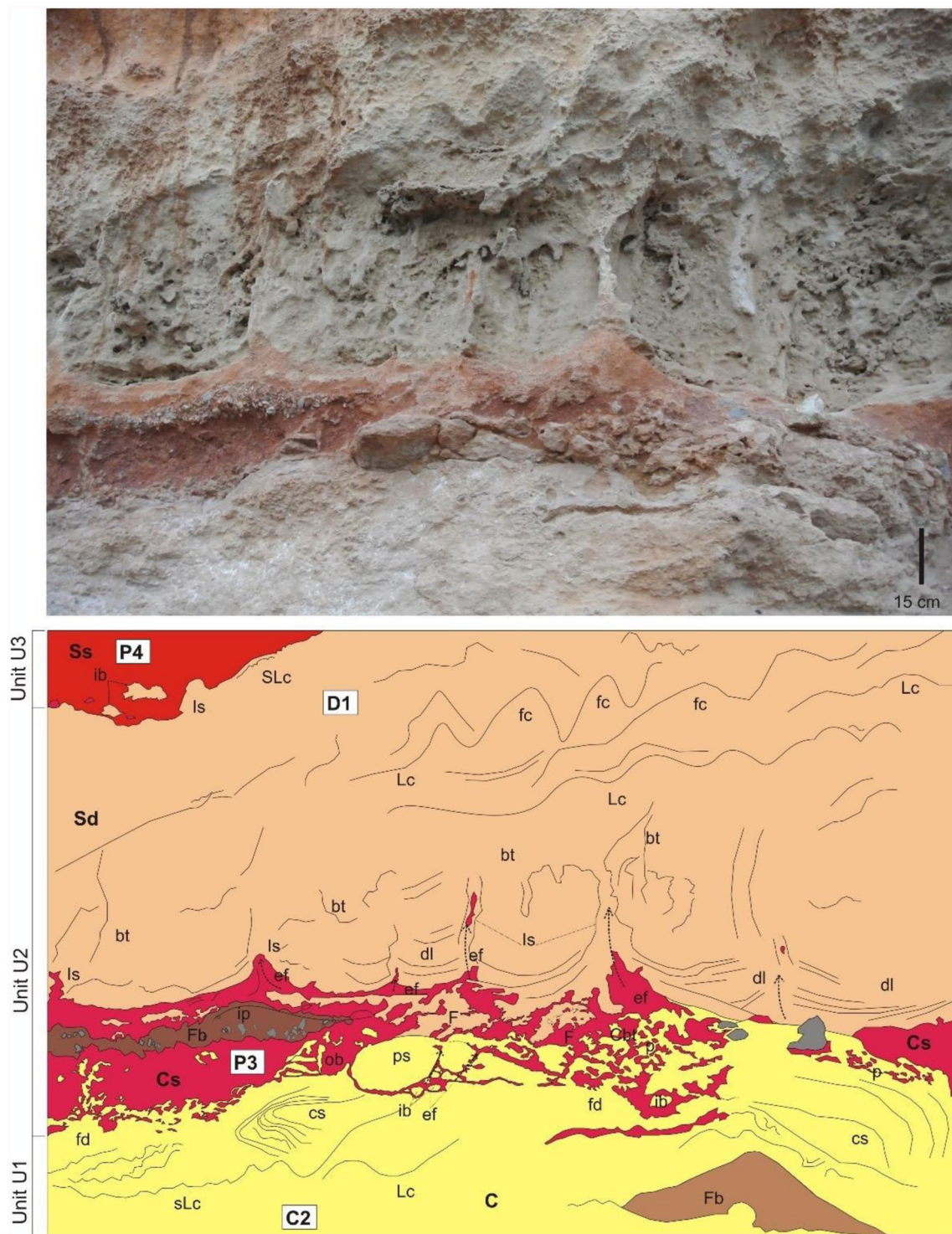
Fig. 5 Picture and drawing of deformed deposits of Es Codolar, illustrating several styles of soft-sediment deformation structures overlain by well-stratified deposits. Large-scale load-cast deformation structure (Ld), small-scale load deformation (sLc), folded lamination / distorted lamination (dl), root casts molds from sandstone bed are filled by silty particles—injection structure (Is), recumbent folds (cs) with parabolic morphology or the axial plane of the folds is sub-horizontal; folded dykes (fd), folded breccia (fb); bioturbation with root casts (bt), extrusive flows (ef), flexi caves (fc), isolated block (ib), imbricated pebbles (ip) oriented block (ob), flames or pillars (F), pseudonodules continuous (ps); cryogenic brecciation (Cbt). Lithological characteristics: sandstone (Sd), marl (Cs), calcretes (C) and silts (Ss)

Injection structures

The injection structures are composed of root cast moulds with a size of 0.50–5 cm width and 15–25 cm height in sandstone levels. They are filled by reddish silts from the underlying palaeosol. The extrusive flows are low marked (ef). The base and upper contact are irregular (Figs. 5 and 6). The analysis of the mineralogical composition carried out both on the lower palaeosol and on the materials that fill the voids—rizoconcretions moulds—of the aeolianites coincide. Conversely, there is no coincidence with the palaeosol located overlying the sandstone layer. These structures occur on two levels; in D1 (Unit U2) and level D2 (Unit U3). Nevertheless, we observed other injection structures within several levels on Cl3 (Unit U1), P4 (Unit U2) and P5 (Unit U3).

Fig. 6 A Injection structure, developed in reddish silts (Cs) filling up the root casts molds presents in the sandstone (Sd). Imbricated pebbles and rocks downslope. Note the presence of bioturbation with abundant root casts (3–5 cm width and 0.5–1 m in height). **B** Detail of the injection structure, folded breccia (Fb), extrusive flows (ef), imbricated pebbles (ib) oriented blocks (ob), complex of vertical, inclined and sub-horizontal dykes (dk), distorted lamination (dl), cryogenic brecciation (Cbt). **C** Detail of injection structure developed in pale brown loamy sands filling up the root casts molds (0.5–5 cm in width and 0.1–0.5 m in height) presents in the sandstone
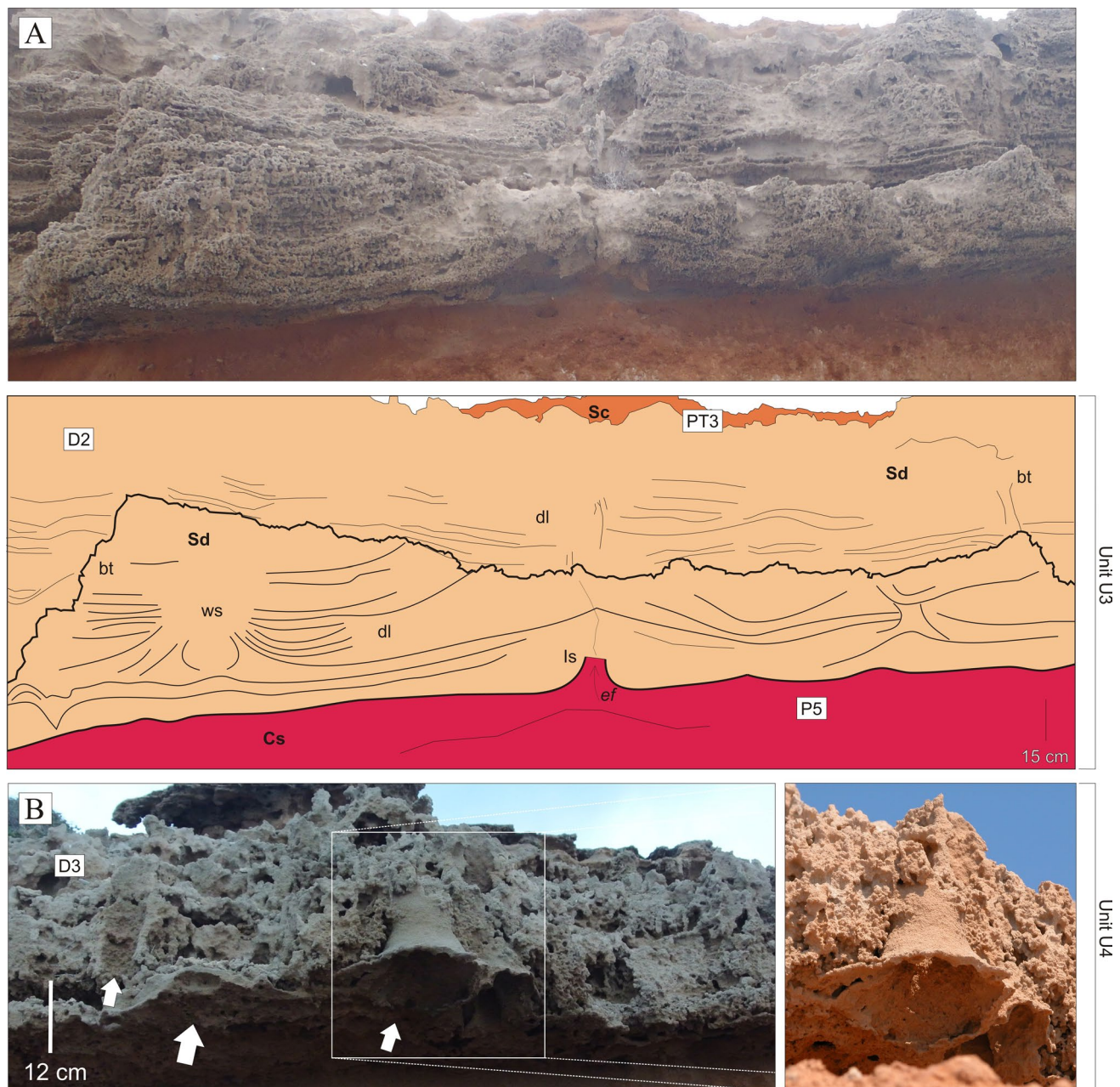
Water-escape structures

The term water-escape structure—hydroplastic mixing layer—is here used in a general sense to include all layers of sediment which have been internally deformed by hydroplastic flowage but which have not moved as a whole relative to surrounding sediments. Internally, liquefaction layers and pockets may show severely deformed primary structures (Fig. 7), nearly complete homogenization, or water-escape structures formed by the redistribution of grains during water-escape and re-sedimentation (Lowe 1975; Trincardi et al. 2004). They are formed when sediment is transported by the expulsion of pore water or gas (Lowe 1975; Owen et al. 2011).

The resulting structures show a range of 15–20 cm in height and 3–25 cm in width. Deformation is limited at the

Fig. 7 **A** Water-escape structure developed in a complete deformed sandstone primary stratified bed; extrusive flows (ef), distorted lamination (dl), folded dykes (dk). **B** Empty volcanoes/bell injection deformed structure developed in a complete deformed sandstone bed. Note the high presence of bioturbation with abundant root casts (0.1–1.5 cm in width and 0.10 to 15–20 cm weight). Lithological characteristics, sandstone (Sd), loamy sands (Sc) and marl (Cs)

top by irregular palaeosol that shows extrusive flows. They are mainly represented by vertical conduits. The vertical development (perpendicular to the primary lamination) is very variable from linear to very irregular. The upper part of the conduits is often represented by conical morphology (wider downward)—like volcanoes—that was probably located at the initial water sediment interface and they end upward with "vent" level. In Fig. 7A, water-escape structures in the sandstone beds forming diapirs or sand volcanoes can be observed. On the other hand, in Fig. 7B, the same structure but completely empty can be observed. These structures are observed in the sandstone levels D2 (Unit U3) and D3 (Unit U4), respectively.

Flames and pillars

Flame structures (Figs. 5 and 8) developed at the interface between sandstone and silts are associated with large-scale load structures (KoçTaşgin et al. 2011). They consist of short, irregular and curved upward protuberances located along sharp boundaries formed between two deformed layers. Flame structures result from diapiric intrusion of fine sediments (Mills, 1983); they formed due to a gravitationally unstable density gradient.

Pillars (Figs. 5 and 8) consist of discrete, straight to slightly sinuous, steeply inclined to vertical paths up to a few centimeters length (usually < 0.10 m) and less than 0.03 m in diameter, which cut sharply through the deformed beds (Rossetti 1999).

Dyke and sill dyke

This structure consists of masses of irregular, convolute laminated or massive sandstone that intruded sharply upwards into the overlying strata to form large (up to 0.65 m long and 0.29 m wide) elongated shapes. Although dykes are morphology similar to pillars, the latter term is reserved to describe discrete, straight to sinuous intrusions, while dykes are larger and show more irregular shapes (Rossetti 1999). The dykes in the study area vary from vertical to steeply dipping and their basal edges attached to underlying sediment sources (Rossetti 1999; Moretti and Sabato 2007).

Ice/sand-wedges

Ice/sand-wedges form by infilling of thermal constriction cracks in permafrost with water or sublimated ice crystal. A key feature of ice-wedge is the occurrence of vertical to steeply dipping laminae generally 0.5–5.0 mm thick (Mackay 1986 in: Murton and Ballantyne 2017; Wolfe et al. 2018). Cross-cutting relationships among laminae are common. Each lamina represents an ice vein formed by the filling of a single thermal contraction crack with ice. Thermal contraction cracks may fill with snow, ice, mineral particles or organic material, producing a variety of vein and wedge-shaped structures characterized as ice-wedges, sand-wedges, soil wedges and composite (ice and sediment) wedges (Murton and Ballantyne 2017). These structures have been observed at the levels P4 and P6; characterized by regular size (1–3 cm height and 10–14 cm width) (Fig. 8).

Collapse structures

The slope collapse in most cases occurs when an area has a steep slope and in the sedimentary succession some lower levels are saturated. The horizontality strata are affected,
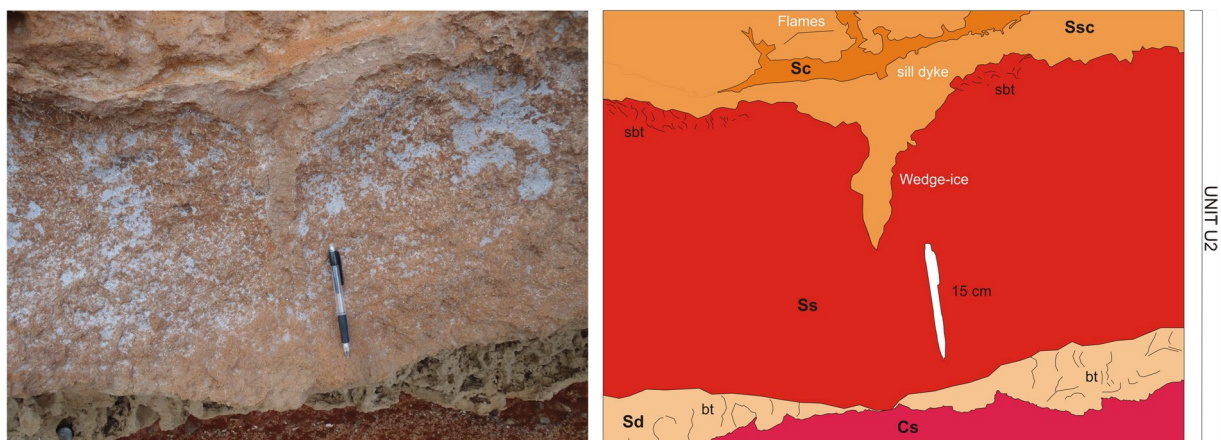
Fig. 8 Picture and line drawing of vertical dykes—Wedge ice, flame and sill dyke observed at the interface between sandstone (Sd) and silts (Ss). The lower sandstone bed (D1) is completed distorted lamination and filled by silt and clay particles (marl) (Cs) level (P3). Note the presence of small root casts (bioturbation) on top level P4

showing the movement of the upper materials due to the plastic behavior of the lower levels, marked by a rupture of the original slope—rugged cut slump. The lower levels are expected to transport the upper ones without affecting the original succession of layers. At the delay of movement derived from the compressive effect of the displacement front, fluids extrude forming cones or cut dikes (Fig. 9). Distinct deformations of this type initiate the movement as result of differences in the hydrostatic gradient (Strachan 2002). Normally, the occurrence of slumps requires the presence of a steep slope (KoçTaşgin et al. 2011).

Others collapse structures are formed when sediment can no longer be supported by its substrate. This may occur in association with karstic solution or substrate weakening (DeMille et al. 1964). The resulting structures can be very diverse (Fig. 10), although they can be overlapped with load structures (Owen et al. 2011).

Cryogenic brecciation

These forms consist of numerous irregular rocks, isolated blocks, or sometimes oriented blocks (Figs. 5, 6 and 10). The blocks have an irregular size generally with 1–5 cm short axis and a 5–15 cm long axis. They are produced by cryoplastic weathering (Lanfranco et al. 2014).

Others associated structures

Depositional structures may be disrupted and distinctive new structures may form as a result of chemical, physical, (e.g., crystal or concretion) and biological processes (e.g., plants roots, footprints) (Fig. 11).

OSL ages

Three OSL ages have been obtained in the Pleistocene succession of Es Codolar. The measured parameters, relevant for age calculation, are presented in Table 1. The samples were collected in aeolian facies beds in order to establish which the main aeolian events that took place here (Fig. 2). The first aeolian level dated corresponds to U2 and shows an age of 317 ± 20 ka, coinciding with the cold stage MIS 10. The next dated sample was from U3 which gave an age of 227 ± 15 ka, coinciding with the cold stage MIS 8. The last one dated was U4; this coincides with the end of the penultimate glacial stage MIS 6 with an age of 124 ± 9 ka (Figs. 12).

Discussion

The sedimentary records of Es Codolar reflect the alternation of Pleistocene cold and warm periods (Del Valle et al. 2016a, b; Del Valle 2016). During the cold periods, sea level dropping led wind-transport inland of the marine sediments exposed on the continental shelf (Fornós et al. 2012a; Andreucci et al. 2014; Del Valle 2016). During the relatively warmer periods, alluvial–colluvial deposits and palaeosols developed (Rose et al. 1999; Muhs et al. 2010; Fornós et al. 2012b; Andreucci et al. 2014; Wagner et al. 2014) and during the interglacial maximums the deposition of beach sediments were the most noticeable (Rose et al. 1999; Andreucci et al. 2010; Bardají et al. 2009; Fornós et al. 2012b; Vicens and Gràcia 2012). The formation of the two types of paleosols have been affected by the environmental conditions of
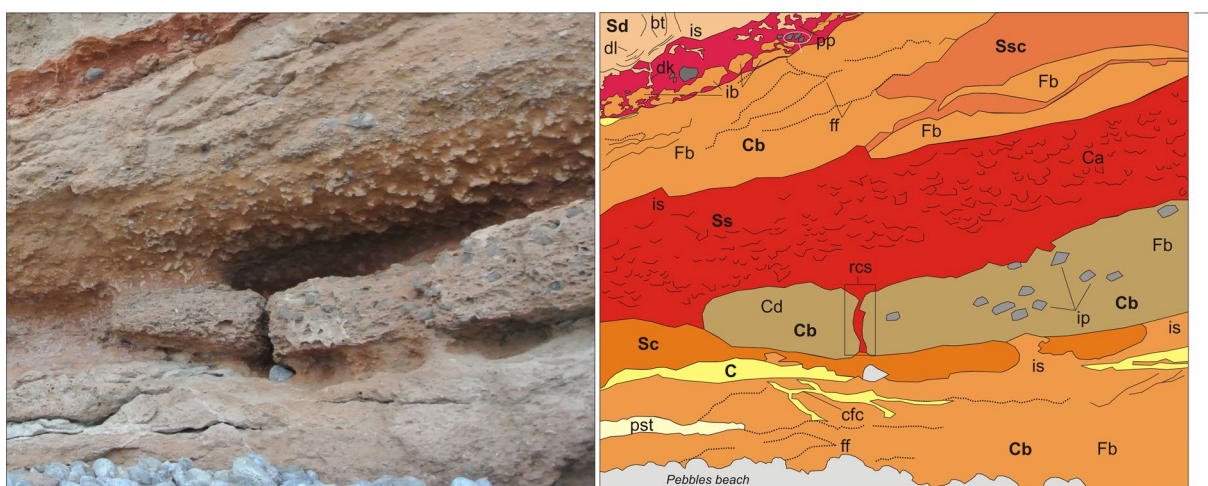
Fig. 9 Picture and line drawing showing slope collapse (rcs) and basal slipping, cut dyke (Cd), injection structure (Is), fractured (ff), pisolits (pst), crack filling with calcretes (cfc), folded breccia (fb), imbricated pebbles (ip), isolated block/pebbles (ib), dykes (dk), pillar or small flame (pp), distorted lamination (dl). Note the presence of bioturbation and carbonate nodules. Lithological characteristics, sandstone (Sd), colluvial (Cb), marl (Ssc, Ss), loamy sands (Sc) and calcretes (C)
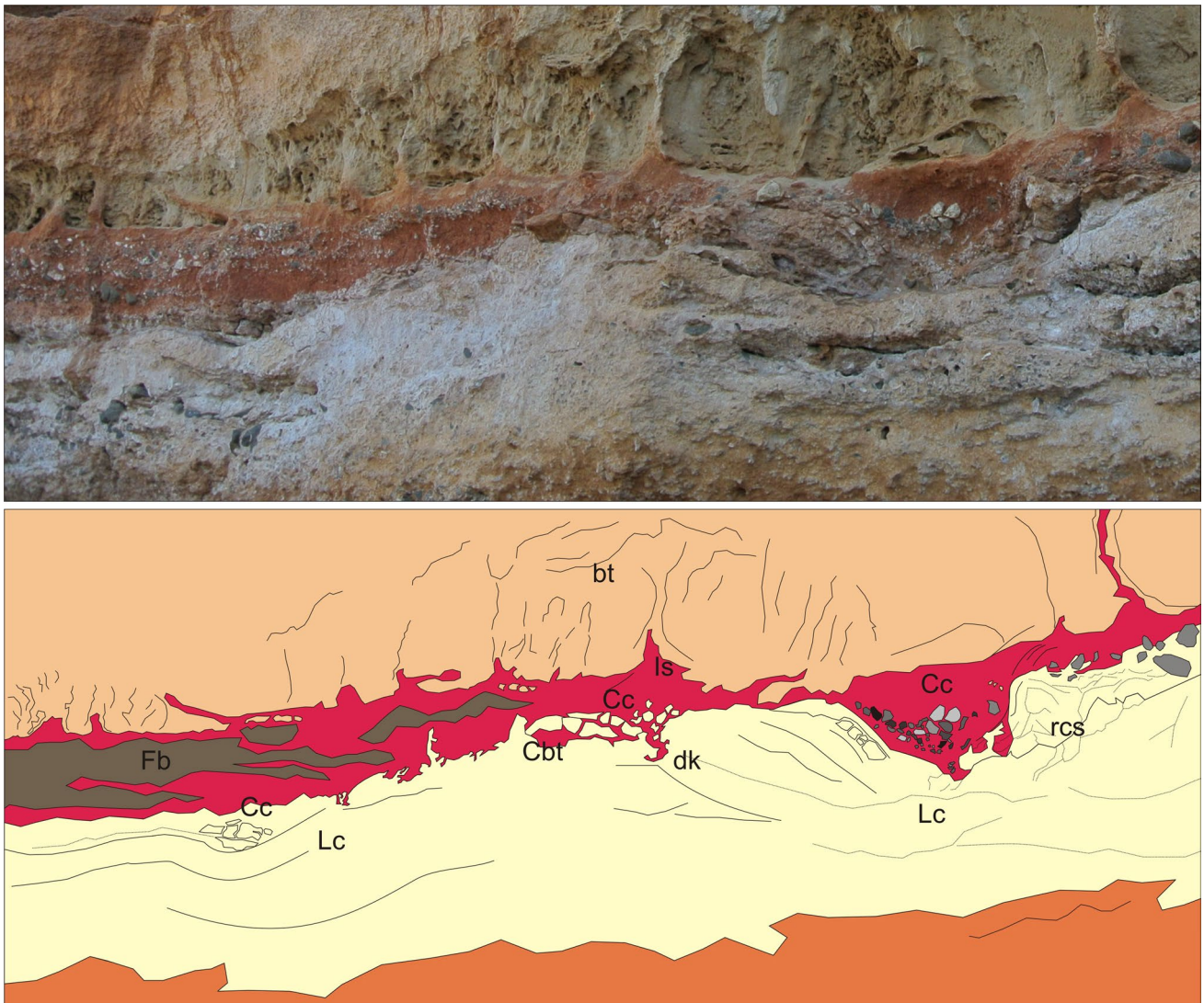
Fig. 10 Picture and line draw of the collapse structure (Cc) associated with the large-scale load structures presence in the outcrops of Es Codolar (Lc); injection structure (Is); slope collapse (rcs), bioturbation (bt), folded breccia (Fb) and dyke (dk); cryogenic brecciation (Cbt)

Fig. 11 **A** Detail picture of the pisolits level. **B** Calcretes of Es Codolar outcrops. **C** Roots casts and root casts molds (5–15 cm in width and 50 cm–1 m in height), the **x** represents two levels with highly small root casts (0.1–2.5 cm in width and 1–10 cm in height approximately)

Table 1 Optically stimulated luminescence dating of Pleistocene aeolianites at Es Codolar (Eivissa)

Sample code		Depth (cm)	Grain size (μm)	Water content (%)	ED (GY)	U-Ra (Bq/Kg)	Th (Bq/kg)	K (Bq/kg)	Total random error (%)	Total Systematic error (%)	Total dose rate (Gy/Ka)	Age (Ka)	MIS
Codolar	M#22#	840	63–250	0.7	154±4 $n=9$	9.8±0.3	4.1±0.2	37.9±2.5	3.27	5.48	0.49±0.01	317±20	10
Eivissa	M#24#	730	63–250	18	100±2 $n=10$	10.1±0.1	3.4±0.1	45.8±3.6	2.97	5.66	0.44±0.01	227±15	8
Profile	M#26#	220	63–250	14.3	59±2 $n=10$	9.8±0.2	3.1±0.3	33.7±3.1	3.93	6.48	0.48±0.01	124±9	6

Summary of the luminescence and dosimetry data used for OSL age calculation. The ages have been obtained using 63–250 μm quartz, with the weighted average values presented here. The uncertainties associated with the equivalent doses and dosimetry (radionuclide specific activities and total dose rates) data are random. n represents the number of aliquots used for equivalent dose estimation. The equivalent dose is computed as the unweighted mean of the equivalent dose distribution. Overdispersion is given. The uncertainties mentioned with the optical ages are the overall uncertainties (random and systematic). Systematic errors include: 2% beta source calibration, 3% conversion factors, 5% attenuation and etching factors, 3% gamma, spectrometer calibration, 15% cosmic radiation. All uncertainties represent 1σ

each moment, that is, for example, the presence of aeolian sediments during a more arid moment contributes to the formation of the silty-sandy soil. Main source of the silty material is arid zones of Northern Africa affected by winds which are able to carry fine particles towards the Balearic Islands and form the majority of the soils (Fornós et al. 1997; Fiol et al. 2005; Muhs 2007).

According to the OSL dating from the aeolian levels, the deposition of coastal dunes of units U2, U3 and U4 took place during the MIS 10, MIS 8 and MIS 6 respectively. This leads us to infer that the colluvial deposits and palaeosols of units U1–U4 were formed during the interglacial stages MIS 11, MIS 9, MIS 7 and MIS 5, respectively.

The study of soft-sediment deformation structures helps us to understand the sedimentary and climatic evolution of Es Codolar sequence. In this sequence, the presence in loamy sandstones beds of ice–sand-wedges at levels P4 and P6 (Fig. 2), located just above the aeolian levels D2 and D3, confirms the occurrence of several periods of cold temperatures just after the deposition, during the glacial stage, of D2 and D3 aeolian levels. But these periods of cold temperatures occurred even during the interglacial stages, as shown by the presence of cryogenic breccias at levels P2 and P3 (located below the D1 aeolian level), deposited during the interglacial stage MIS 11.

On the other hand, in Es Codolar sequence, the soft-sediment deformation structures are considerably larger and frequent into the lower levels than into the upper levels, pointing to an increasing load as responsible for the development of these structures. In this way, structures formed after the deposition of the majority of the sedimentary levels. Moreover, because the liquefaction structures formed in water-saturated sediments, it is more probable than these structures were formed during the interglacial stages, when sea level is higher, the rainfall increase and therefore, there is a greater presence of vegetation. In Fig. 1, a coastal lagoon is observed near the outcrop, indicating the significant proximity of the water table. Thus, in Es Codolar, during the interglacial stages the sediments were saturated due to both a wetter environment and a higher water table, being the maximum high during MIS 5, when sea level was nearly 3 m higher than today (Polyak et al. 2018). Because of these two reasons (1st—maximum sea level during MIS 5, and 2nd—deformation structures larger and more frequent at the lower levels), we infer that the soft-sediment deformation structures were formed at the end of MIS 6 to MIS 5, after the deposition of aeolian unit U4.

Based on the discussion above, Fig. 12 shows the evolution of the Pleistocene sedimentary sequence of Es Codolar. After the formation of the colluvial beds at the base of the sequence, the first aeolian level was deposited during a relative sea level drop in MIS 10 (Fig. 13). Bioturbation structures developed in this level, with dominant palaeo-wind
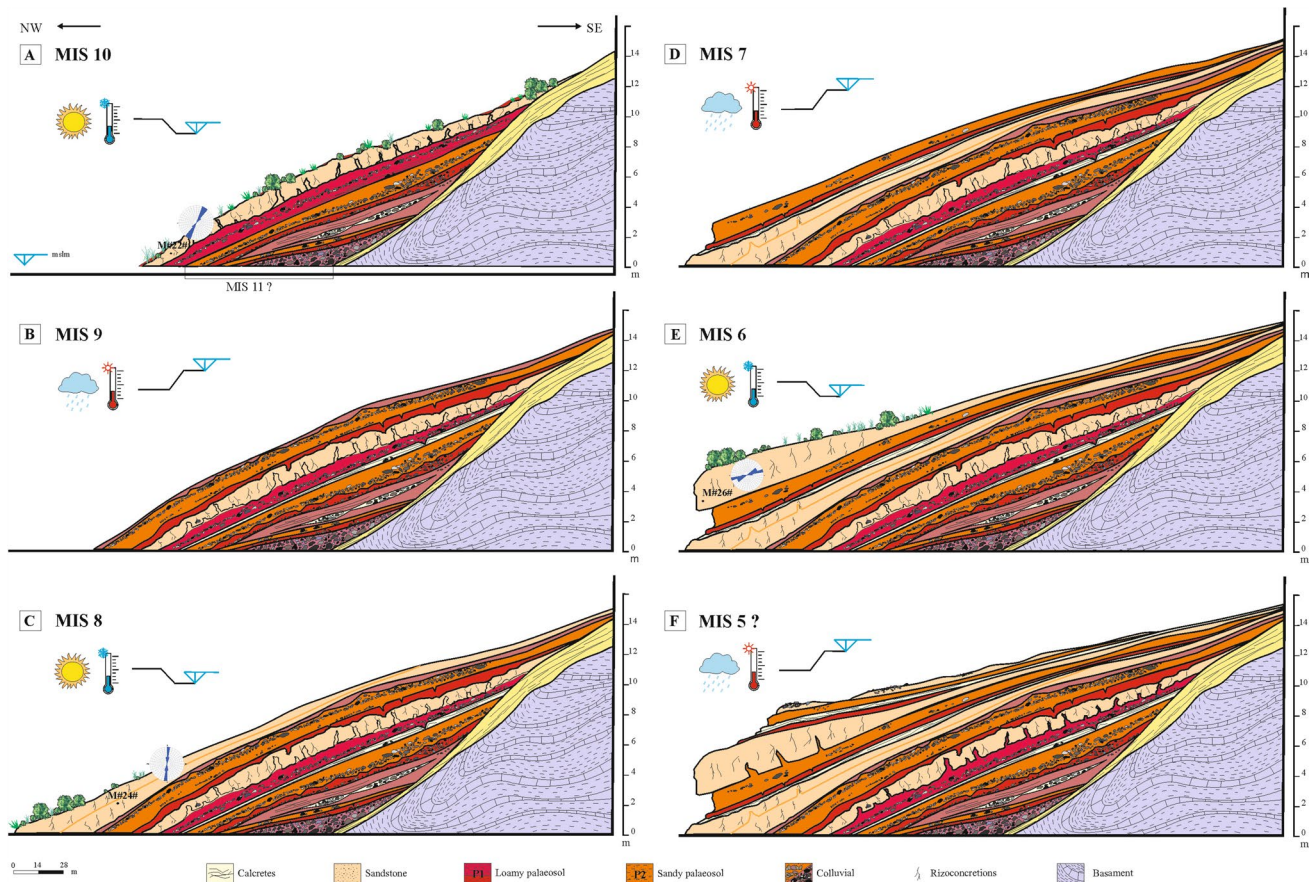
Fig. 12 Depositional environment evolution model showing the succession of the main sedimentary environments, paleocurrent directions of the western coast of Eivissa from MIS 10 to MIS 5 and the soft-sediment deformations

currents from SSW to NNE (Fig. 12A). During MIS 9, a thin sequence (1 m) of colluvial and palaeosol sediments was deposited on top of the previous aeolian level. A second aeolian level was formed during MIS 8 under a predominant wind from S to N. Bioturbation structures also developed into this level (Fig. 12c). During MIS 7, characterized by a higher water level and humidity than in MIS 6 (Fig. 13), a thin sandy palaeosol was formed, with some intercalation of colluvial beds (Fig. 12d). The upper aeolian level was emplaced during MIS 6 and has the same characteristics as the previous aeolian beds. At the end of this period soft sedimentary deformation structures formed. These structures are larger and frequent in lower levels because of the increasing load as we go lower in the stratigraphic series. The sequence of Es Codolar ends with the deposition of a thin sequence of sandy and loamy palaeosols and calcretes corresponding to MIS 5. This combined with an intensification in the pluviometry and the rise of the water table, produced fluidization structures of these palaeosol into the upper aeolian level.

Conclusions

Results of sedimentary analyses and OSL dating allowed distinguishing the effects of climatic fluctuations during the sedimentation of these Pleistocene deposits. Due to the strong climatic signal registered in Es Codolar sequence and the absence of significant tectonic movement, changes in the environmental agents (i.e., arid-wetter periods and sea level changes) are the most plausible processes controlling the described sediment deformations. The common factor in the formation of soft-sediment structures is that all the origin sediments went through liquefaction–fluidization, which appears to be mostly triggered by a combination of sea level rise and increasing humidity during interglacial periods. It should not be forgotten, however, that wave erosion at the hillslope could also contribute to instability of the outcrop. On the other hand, during glacial periods, the encroaching of new dune fields on Es Codolar added up thick sedimentary bodies to the outcrop package that could have increased the overloading processes. The colder conditions during these periods could have boosted the cryogenic-related structures, which help
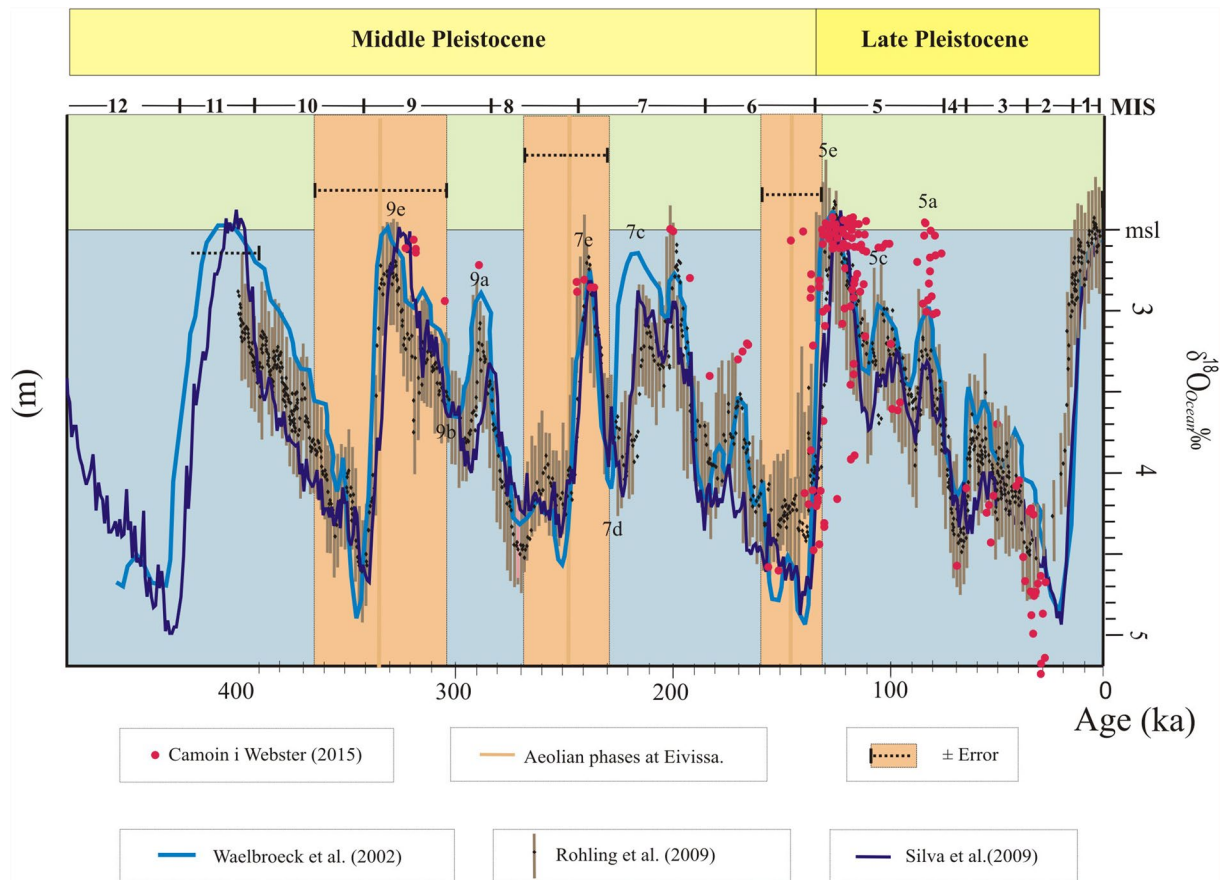
Fig. 13 Sea level reconstructions for the last 500 Ka based on continuous records of O^{18} benthic by Silva et al. (2009); sea level reconstructions for the last 500 Ka based on continuous records, compiled from the Red Sea by Rohling et al. (2009, 2012); O^{18} benthonic registers present in the deep waters of Waelbroeck et al., (2002); coral reefs register for Camoin and Webster (2015) and representation of the periods of aeolian sedimentation on the island of Ibiza based on the absolute OSL dating performed here, shaded in pale brown. The black line symbols represent the OSL age ± error

us in the understanding of the climatic evolution and the syn- and post-depositional processes. The main processes triggering the formation of these structures seem to be sea level changes together with a wetter environment during warmer climatic episodes.

References

Adamiec G, Aitken MJ (1998) Dose-rate conversion factors: update. Ancient TL 16:37–50

Allen JRL (1982) Sedimentary structures: their character and physical basis, vol II. Elservier, New York, p 663

Andreucci S, Clemmensen LB, Murray A, Pascucci V (2010) Middle Late Pleistocene coastal deposits of Alghero, northwestern Sardinia (Italy): chronology and evolution. Quatern Int 222:3–16

Andreucci S, Panzeri L, Martini P, Maspero F, Martini M, Pascucci V (2014) Evolution and architecture of a West Mediterranean Upper Pleistocene to Holocene coastal apron-fan system. Sedimentology 61:333–361

Anechitei-Deacu V, Timar-Gabor A, Constantin D, Trandafir-Antohi O, del Valle L, Fornós JJ, Gómez-Pujol L, Wintle AG (2018) Assessing the maximum limit of SAR-OSL dating using quartz of different grain sizes. Geochronometria 45(1):146–159. https://doi.org/10.1515/geochr-2015-0092

Bardají T, Goy JL, Zazo C, Hillaire-Marcel C, Dabrio CJ, Cabero A, Ghaleb B, Silva PG, Lario J (2009) Sea level and climate changes during OIS 5e in the Western Mediterranean. Geomorphology 104:22–37

Brenchely PJ, Newall G (1977) The significance of contorted bedding in the Upper Ordovician sediments of the OSLO region, Norway. J Sedimentol Petrol 47:819–833

Camoin GF, Webster JM (2015) Coral reef response to Quaternary sea-level and environmental changes: State of Science. Sedimentology 62:401–428. https://doi.org/10.1111/sed.12184

Chan A, Bruhn L (2014) Dynamic liquefaction of Jurassic sand dunes: processes, origins, and implications. Earth Surf Proc Land 39:1478–1491

Clemmensen LB, Lisborg T, Fornós JJ, Bromley RG (2001) Cliff-front aeolian and colluvial deposits, Mallorca, Western Mediterranean: a record of climatic and environmental change during the last glacial period. Bull Geol Soc Den 48:217–232

Del Valle L (2016) El registre sedimentari eòlic del Plistocèlitoral d'Eivissa. PhD thesis, Universitat de les Illes Balear

Del Valle L, Fornós JJ, Gómez-Pujol L, Pomar F, Anechitei-Deacu V, Timar-Gabor A (2015) El Pleistoceno medio de la zona de Cala Bassa (Eivissa, Mediterráneo Occidental): Evolución paleoclimática. Geotemas 15:169–172

Del Valle L, Gómez-Pujol L, Fornós JJ, Timar-Gabor A, Anechitei-Deacu V, Pomar F (2016a) Middle to Late Pleistocene dunefields in rocky coast settings at Cala Xuclar (Eivissa, Western Mediterranean): Recognition, architecture and luminescence chronology. Quatern Int 407:4–13

Del Valle L, Pomar F, Fornós JJ, Gómez-Pujol L (2016b) Estructuras de deformación de la secuencia sedimentaria pleistocena costera de Es Codolar (Eivissa, Mediterráneo occidental). Geotemas 17:15–18

DeMille G, Shouldice JR, Nelson NW (1964) Collapse structures related to the Prairie Formation, Saskatchewan. Geol Soc Am Bull 75(4):307–316

Diaz de Neira A, Garcia de Domingo A, Gil I, Cabra P, Ruíz P (1997) Mapa Geológico de España. Escala 1:200.000. Ibiza 65/09-08. Instituto Geológico y Minero de España, Madrid

Dorale JA, Onac PB, Fornós JJ, Ginés J, Ginés A, Tuccimei P, Peate DW (2010) Sea-level highstand 81,000 years ago in Mallorca. Science 327:860–863

Downs RT, Hall-Wallace M (2003) The American mineralogist crystal structure data base. Am Miner 88:247–250

El-Asmar H (1994) Aeoloianite sedimentation along the northwestern coast of Egypt: evidence for middle to late quaternary aridity. Quatern Sci Rev 13:699–708

Ezquerro L, Moretti M, Liesa CL, Luzón A, Pueyo EL, Simón JL (2016) Control son space-time distribution of Soft-sediment deformation structures: applying palaeomagnetic dating to approach the apparent recurrence period of paleoseisms at the Conard Fauld (eastern Spain). Sed Geol 344:91–111

Fiol Ll, Fornós JJ, Gelabert B, Guijarro JA (2005) Dust rains in Mallorca (Western Mediterranean): their occurrence and role in some recent geological processes. CATENA 63(1):64–84

Fornós JJ, Crespí D, Fiol LA (1997) Aspectes mineralògics i texturals de la pols procedents de les plugues de fang a les Illes Balears: la seva importancia en alguns processos geològics recents. Bolletí De La Societat D'història Naturalde Les Balears 40:113–122

Fornós JJ, Clemmensen LB, Gómez-Pujol L, Murray A (2009) Late Pleistocene carbonate aeolianites on Mallorca, Western Mediterranean: a luminescence chronology. Quatern Sci Rev 28:2697–2709

Fornós JJ, Clemmensen LB, Gómez-Pujol L, Ginés A, Ginés J (2012a) Pleistocene eolianites and low sea levels. A field trip. In: Ginés A, Ginés J, Gómez-Pujol L, Onac BP, Fornós JJ (eds) Mallorca: A Mediterranean benchmark for quaternary studies, vol 18. Mon Soc Hist Nat Balears, pp 85–110

Fornós JJ, Ginés A, Ginés J, Gòmez-Pujol L, Gràcia F, Merino A, Onac BP, Tuccimei P, Vicens D (2012b) Upper Pleistocene deposits and karst features in the littoral landscape of Mallorca Island (Western Mediterranean): a field trip. In: Ginés A, Ginés J, Gómez-Pujol L, Onac BP, Fornós JJ (eds) Mallorca: a Mediterranean benchmark for quaternary studies, vol 18. Mon. Soc. Hist. Nat. Balears, pp 163–220

Gil J, García de Domingo A, Díaz de Neira A, Cabra P (1997) Mapa Geológico de Ibiza y Formentera a escala 1:100.000 (Geológico de Ibiza-Formentera 100)

Hansen V, Murray A, Buylaert JP, Yeo EY, Thomsen KJ (2015) A new irradiated quartz for beta source calibration. Radiat Meas 81:123–127

Horváth Z, Michéli E, Mindszenty A, Berényi-Üveges J (2005) Soft-sediment deformation structures in Late Miocene-Pleistocene sediments on the pediment of the Mátra Hills (Visonta, Atkár, Verseg): cryoturbation, load structures or seismites? Tectonophysics 410:81–95

Just J, Hübscher C, Betzler C, Lüdmann T, Reicherter K (2011) Erosion of continental margins in the Western Mediterranean due to sea-level stagnancy during the Messinian salinity crisis. Geo-Mar Lett 31:51–64

KoçTaşgin CK, Orhan H, Tükmen I, Aksoy E (2011) Soft-sediment deformation structures in the late Miocene Şelmo Formation around Adiyaman area, Southeastern Turkey. Sed Geol 235:277–291

LanFranco M, Rapisardi E, Giardino M (2014) A missed window of opportunity. Chapter 36. 185 to 190 In: Lollino G, Arattano M, Oliveira R, Peppoloni S (eds) Engineering Geology for Society and Territory—V. 7: Education, professional ethics and public recognition of engineering geology. Springer, Berlin

Lowe DR (1975) Water-escape structures in coarse grained sediments. Sedimentology 22:157–204

Lowe DR (1976) Subaqueous liquefied and fluidized sediment flows and their deposits. Sedimentology 23:285–308

Maltman AJ (1994) The geological deformation of sediments. Chapman and Hall, London

Martrat B, Grimalt JO, López-Martínez C, Cacho I, Sierro FJ, Flores JA, Zahn R, Canals M, Curtis JH, Modell DA (2004) Abrupt temperature changes in the Western Mediterranean over the past 250,000 years. Science 306:1762–1765

Mills PC (1983) Genesis and diagnòstic value of soft-sediment deformation structures- a review. Sed Geol 35:83–104

Molina JM, Alfaro P, Moretti M, Soria JM (1998) Soft-Sediment deformation structures induced by cyclic stress of storm waves intempestites (Miocene, Guadalquivir basin, Spain). Terra Nova 10:145–150

Moretti M (2000) Soft-sediment deformation structures interpreted as seismites in middle-late Pleistocene aeolian depòsits (Apulian foreland, Southern Italy). Sed Geol 135:167–179

Moretti M, Sabato L (2007) Recognition of trigger mechanisms for soft-sediment deformation in the Pleistocene lacustrine deposits of the Sant Arcangelo Basin (Southern Italy): Seismic shock vs. Overload Sediment Geol 196:31–45

Muhs DR, Budahn J, Avila A, Skipp G, Freeman J, Patternson D (2010) The role of African dust in the formation of Quaternary soils on Mallorca, Spain and implications for the genesis of Red Mediterranean soils. Quatern Sci Rev 29:2518–2543

Muhs D (2007) Paleosols and wind-blown sediments: overview. In: Encyclopedia of quaternary science. Elsevier, Amsterdam. https://doi.org/10.1016/B0-44-452747-8/00378-1

Murray AS, Clemmensen LB (2000) Luminescence dating of Holocene aeolian sand movement, Thy, Denmark. Quatern Sci Rev 20:751–754

Murray AS, Wintle AG (2003) The single aliquot regenerative dose protocol: potential for improvements in reliability. Radiat Meas 37:377–381

Murton JB, Ballantyne CK (2017) Periglacial and permafrost ground models for Great Britain. In: Gniffths JS, Martin CJ (eds) Engineering geology and geomorphology of glaciated and periglaciated terrains—Engineering Group Working Party Report. Engineering Geology Special Publications 28. Geological Society, London, pp 501–597. https://doi.org/10.1144/EGSP28.5

Nielsen KA, Clemmensen LB, Fornós JJ (2004) Middle Pleistocene magnetostratigraphy and susceptibility stratigraphy: data from a carbonate aeolian system, Mallorca, Western Mediterranean. Quatern Sci Rev 23:1733–1756

Olabode S (2014) Soft sediment deformation structures in the Maastrichtian. Ajali Formation, Western Flank of Amambrer Basin, Southern Nigeria. J Afr Earth Sci 89:16–30

Owen G (1996) Experimental soft-sediment deformations: structures formed by liquefaction of unconsolidated sands and some ancient examples. Sedimentology 43:279–293

Owen G (1987) Deformation processes in unconsolidated sands In: Jones ME, Preston RMF (eds) Deformation of sediments and sedimentary rocks. Geological Society, London, Special Publication No. 29, pp 11–24

Owen G, Moretti M, Alfaro P (2011) Recognizing triggers for soft-sediment deformation: current understanding and futur directions. Sed Geol 235:133–140

Pappalardo M, Chelli A, Ciampalini A, Rellini I, Biagioni F, Brückner H, Fülling A, Firpo M (2013) Evolution of an Upper Pleistocene aeolianite in the northern Mediterranean (Liguria, NW Italy). Ital J Geosci 132(2):290–303

Polyak VJ, Onac BP, Fornós JJ, Hay C, Asmerom Y, Dorale JA, Ginés J, Tuccimei P, Ginés A (2018) A highly resolved record of relative sea level in the western Mediterranean Sea during the last interglacial period. Nat Geosci 11:860–864. https://doi.org/10.1038/s41561-018-0222-5

Pomar F (2016) Arquitectura i fàcies deposicionals de la interferència entre la sedimentació al·luvial, col·luvial i eòlica a les Illes Balears durant el Pleistocè Superior: Implicacions paleoclimàtiques. PhD Thesis

Pomar F, Del Valle L, Fornós JJ, Gòmez-Pujol L (2015) Registro sedimentario Litoral del Pleistoceno en las Islas Baleares (Mediterráneo Occidental): implicaciones paleoclimáticas. VIII Jornadas De Geomorfología Litoral. Geotemas 15:65–68

Prescott JR, Hutton JT (1994) Cosmic ray contributions to dose rates for luminescence and ESR dating: large depths and long terms variations. Radiat Meas 23(2–3):497–500

Rangheard Y (1971) Etude géologique des îles d'Ibiza et de Formentera (Baléares). Mem IGME 82:1–340

Rohling EJ, Grant K, Bolshaw M, Roberts AP, Siddall M, Hemleben C, Kucera M (2009) Antarctic temperature and global sea level closely coupled over the past five glacial cycles. Nat Geosci 2:500–504. https://doi.org/10.1038/ngeo557

Rohling EJ, Sluijs A, Dijkstra HA, van de Wal RSW, von der Heydt AS, Bijl PK, Zeebe R (2012) Making sense of palaeoclimate sensitivity. Nature 491:683–691. https://doi.org/10.1038/nature11574

Rose J, Meng X, Watson C (1999) Palaeoclimate and palaeoenvironmental responses in the western Mediterranean over the last 140 ka: evidence from Mallorca, Spain. J Geol Soc Lond 156:435–448

Rossetti DF (1999) Soft-sediment deformation structures in late Albian to Cenomanian depòsits, São Luís Basin, northen Brazil: evidence for palaeoseismicity. Sedimentology 46:1065–1081

Sàbat F, Gelabert B, Rodríguez-Perea A, Jiménez J (2011) Geological structure and evolution of Majorca: Implications for the origin of the western Mediterranean. Tectonophysics 510:217–238

Shillizzi R, Luna L, Falco JI (2010) Estructuras de deformación (¿Sismitas?) en la formación río Negro, provincia de río Negro, Argentina. Lat Am J Sedimentol Basin Anal 17(1):17–32

Silva PG, Zazo C, Bardají T, Baena J, Lario J, Rosas A, Van der Made, J (2009) Tabla cronostratigràfica del Cuaternario de la Península Ibérica, v.2. AEQUA. www.aequa.es. Accessed 2 Oct 2018

Strachan L (2002) Slump initiated and controlled syndepositional sandstone removilization: and exemple from the Namurian of Country Clare, Ireland. Sedimentology 49:25–41

Thomsen KJ, Bøtter-Jensen L, Denby P, Moska P, Murray AS (2006) Developments in luminescence measurements techniques. Radiat Meas 41:768–773

Trincardi F, Cattaneo A, Correggiari A, Ridente D (2004) Evidence of soft sediment deformation, fluid escape, sediment failure and regional weak layers within the late Quaternary mud deposits of the Adriatic Sea. Mar Geol 213:91–119

Vicens D, Gràcia F (2012) Quaternary beach deposits in Mallorca: paleontological and geormorphological data. In: Ginés A, Ginés J, Gómez-Pujol L, Onac BP, Fornós JJ (eds) Mallorca: a Mediterranean benchmark for quaternary studies, vol 18. Mon. Soc. Hist. Nat. Balears, pp 55–83

Waelbroeck C, Labeyrie L, Michel E, Duplessy JC, Mcmanus JF, Lambeck K, Balbon E, Labracherie M (2002) Sea-level and deep-water temperature change derived from benthic foraminifera isotopic records. Quatern Sci Rev 21:295–305

Wagner S, Eckmeier E, Skowronek A, Günster N (2014) Quaternary paleosols and sediments on the Balearic Islands as indicators of climate changes. CATENA 112:112–124

Wolfe S, Morse PD, Neudorf C, Kokelj SV, Lian OB, O'Neill HB (2018) Contemporary sand wedge development in seasonally frozen ground and paleoenvironmental implications. Geomorphology 308:215–229

Zazo C (1999) Interglacial sea levels. Quatern Int 55:101–113